

# On the parametrization of the distributions of depth of shower maximum of ultra-high energy extensive air showers

Luan B. Arbeletche and Vitor de Souza

*Instituto de Física de São Carlos, Universidade de São Paulo,*

*Av. Trabalhador São-carlense 400, São Carlos, Brasil.*

(Dated: February 27, 2022)

## Abstract

The distribution of depth in which a cosmic ray air shower reaches its maximum number of particles ( $X_{\max}$ ) is studied and parametrized. Three functions are studied for proton, carbon, silicon, and iron primary particles with energies ranging from  $10^{17}$  eV to  $10^{20}$  eV for three hadronic interaction models: EPOS-LHC, QGSJETII.04, and SIBYLL2.3C. The function which best describes the  $X_{\max}$  distribution of a mixed composition is also studied. A very large number of simulated showers and a detailed analysis procedure are used to guarantee negligible effects of undersampling and of fitting in the final results. For the first time, a comparison of several functions is presented under the same assumption with the intention of selecting within them the best functional form to describe the  $X_{\max}$  distribution. The Generalized Gumbel distribution is shown to be the best option among the options for a general description of all cases. The Log-normal distribution is also a good choice for some cases while the Exponentially Modified Gaussian distribution has shown to be the worst choice in almost all cases studied. All three functions are parametrized as a function of energy and primary mass.

**Note on this version:** an update to the parametrization discussed in Section V and whose parameters are tabulated in Appendix B has been added as Appendix C. This update envisages the inclusion of Helium primaries in the simulation library, which results in an improved description of the  $X_{\max}$  distributions for masses in the range  $A = 1$  to  $A = 12$ . For details on the method and the functional form of the new parametrization, refer to Section V; these two aspects remain unchanged. The new values of the parametrization coefficients and their statistical uncertainties can be found in Appendix C. We thank Olena Tkachenko for calling our attention to the need of including helium primaries for a better description of all elements.

## I. INTRODUCTION

The relative abundance of particle compositions in ultra-high energy cosmic rays (UHECR) is of key importance in the understanding of their acceleration mechanisms and interactions with extra-galactic radiation fields. The maximum particle energy of each source, the probability of escape from the acceleration region, the luminosity of the sources classes, the mean free path of the interaction on the way to Earth and the deviation angle in the magnetic fields are examples of fundamental astrophysics phenomena which depend on the particle type (mass and/or charge). A major improvement in our understanding of UHECR physics will not be possible without a precise determination of the abundance of each particle type. With this in mind, the two most important UHECR observatories (The Pierre Auger and the Telescope Array Observatories) are implementing upgrades to enhance their capabilities to determine the relative abundances of particle types arriving on Earth.

At these energies, the particles hitting Earth, called primary particles, are not directly observed. Their interaction with the atmosphere generates a cascade of particles which is measured by telescopes and ground detectors. The properties of the primary particle can be reconstructed from the detected signal of the shower. The most used and reliable parameter to determine the primary particle type is the depth at which the cascade reaches its maximum number of particles ( $X_{\text{max}}$ ). These extensive air showers are very complex branching processes whose stochastic behavior, although well understood in terms of particle interaction processes, cannot be solved analytically. Thus, fluctuations of important global quantities such as  $X_{\text{max}}$  have no known functional form. In this sense, one always has to rely on Monte Carlo simulations to understand the intrinsic fluctuations of extensive air showers. Moreover, an approximation to the functional form of global variables can only be determined by the parametrization of simulated quantities.

Constant improvements in the fluorescence technique have allowed the Pierre Auger Observatory to measure  $X_{\text{max}}$  with a systematic uncertainties of about  $\pm 8 \text{ g/cm}^2$  [1] and the TA Collaboration quotes systematic uncertainties of  $\pm 17.4 \text{ g/cm}^2$  [2]. The resolution in  $\langle X_{\text{max}} \rangle$  are quoted to be smaller than  $25 \text{ g/cm}^2$  for the Pierre Auger Observatory measurements. The precision in measuring  $X_{\text{max}}$  is such that new studies are based on the full distribution instead of only its moments [1–5].

In this context, a good understanding of the  $X_{\text{max}}$  distribution shape is mandatory since

many steps in the analysis procedures depend on knowing *a priori* its expected shape. The adoption of a particular parametrization may cause a wrong interpretation of  $X_{\max}$  distributions when studying the primary fractions and their evolution with energy. Some functions have been proposed to describe the  $X_{\max}$  distribution [6, 7] but no comparison between them is available. In this paper, three functions are used to describe the  $X_{\max}$  distribution and a detailed statistical comparison between them is presented. The purpose of this paper is to select the best description of the  $X_{\max}$  distribution and parametrize its dependencies with energy and mass.

This study is based on Monte Carlo simulations of air shower which are discussed in section II. In section III, the functions used to describe the  $X_{\max}$  distribution are presented and discussed. Section IV presents the results of the fits and section VI presents the conclusions.

## II. SIMULATION OF $X_{\max}$ DISTRIBUTIONS

Large samples of extensive air showers are simulated using the software CONEX [8]. This software is an implementation of a one-dimensional hybrid model of the longitudinal development of particle cascades which has been extensively tested [6]. Four atomic nuclei are considered: proton, carbon, silicon and iron ( $A = 1, 12, 28$  and  $56$ , respectively) with energies ranging from  $10^{17}$  eV to  $10^{20}$  eV in steps of 1 in  $\log_{10}(E_0/\text{eV})$ . The incident zenith angle of the primary cosmic rays is set to  $75^\circ$ . The longitudinal development is sampled in steps of  $10 \text{ g/cm}^2$  until particles reach sea level, corresponding to a slant depth of  $3860 \text{ g/cm}^2$ . The energy cutoff for hadrons, muons, electrons, and photons is 1 GeV, 1 GeV, 1 MeV and 1 MeV, respectively. Given the known dependence on hadronic interaction models [9–11], three post-LHC hadronic interaction models are considered: EPOS-LHC [12], QGSJETII.04 [13] and SIBYLL2.3C [14]. For each combination of primary mass, energy and hadronic interaction model,  $10^6$  showers are simulated.

CONEX provides the depth at which a shower reaches its maximum number of particles (XMX variable in CONEX output) and the depth at which the energy deposit profile reaches its maximum (XMXDEdX in CONEX output). XMX and XMXDEdX are calculated by fitting a quadratic function around the maximum of the longitudinal particle and energy deposit profile, respectively. Details of the fitting procedure can be found in the CONEX manual [8]. These variables are compared and a maximum difference of  $0.8 \pm 3.4 \text{ g/cm}^2$

between them is found in all simulated cases. Given that the difference between these variables is very small, much smaller than the uncertainties of the measurements, the depth at which the shower reaches the maximum number of particles ( $X_{MX}=X_{\max}$ ) is used in the following calculations. The small difference and statistical uncertainty between  $X_{MX}$  and  $X_{MXDEDX}$  also illustrate the quality of the fit done in CONEX.

Showers with two maxima in the longitudinal profile, the so-called double bump showers [15], for which the depth of shower maximum is not an unambiguously defined quantity, are removed from our analysis. The double bump showers are identified by searching the longitudinal profiles with more than two inflection points by computing the second derivative of profiles at each point in terms of finite differences. This approach effectively removes showers with two pronounced peaks. The fraction of removed profiles is below 0.4% for all combinations of primary, energy and hadronic model.

Examples of simulated  $X_{\max}$  distributions for some primary masses with energies of  $10^{17}$  eV (upper panel) and  $10^{20}$  eV (lower panel) are shown in figure 1. Primary types are indicated in the top-right corner of each plot. Each colored line corresponds to simulations done with a particular hadronic interaction model, indicated in the legend of the left plots. These distributions, as already known, have an accentuated positive skew that results from the exponential nature of particle interaction length distributions. Note, in figure 1, the logarithm scale in the y-axis and the very small fluctuations of each point. In this illustration,  $X_{\max}$  was binned in intervals of  $10 \text{ g/cm}^2$ . As a result from the large simulated samples, fluctuations in the obtained distributions become larger only for very deep showers.

### III. PROPOSED FUNCTIONS TO DESCRIBE THE $X_{\max}$ DISTRIBUTIONS

In this section, three functions are studied to parametrize the  $X_{\max}$  distributions: Exponentially Modified Gaussian, Generalized Gumbel, and Log-normal. They are going to be explained below and, whenever possible, an interpretation of their parameters is going to be given. Other functions have also been tested: Amoroso, Lévy  $\alpha$ -stable, Fréchet, Exponentiated Fréchet, Exponentiated Exponential, Landau and Gamma, but either they do not showed a good description of the  $X_{\max}$  distributions or they unreasonably increased the number of fitting parameters without providing a better description of data. The motivation for each function is also going to be briefly explored.

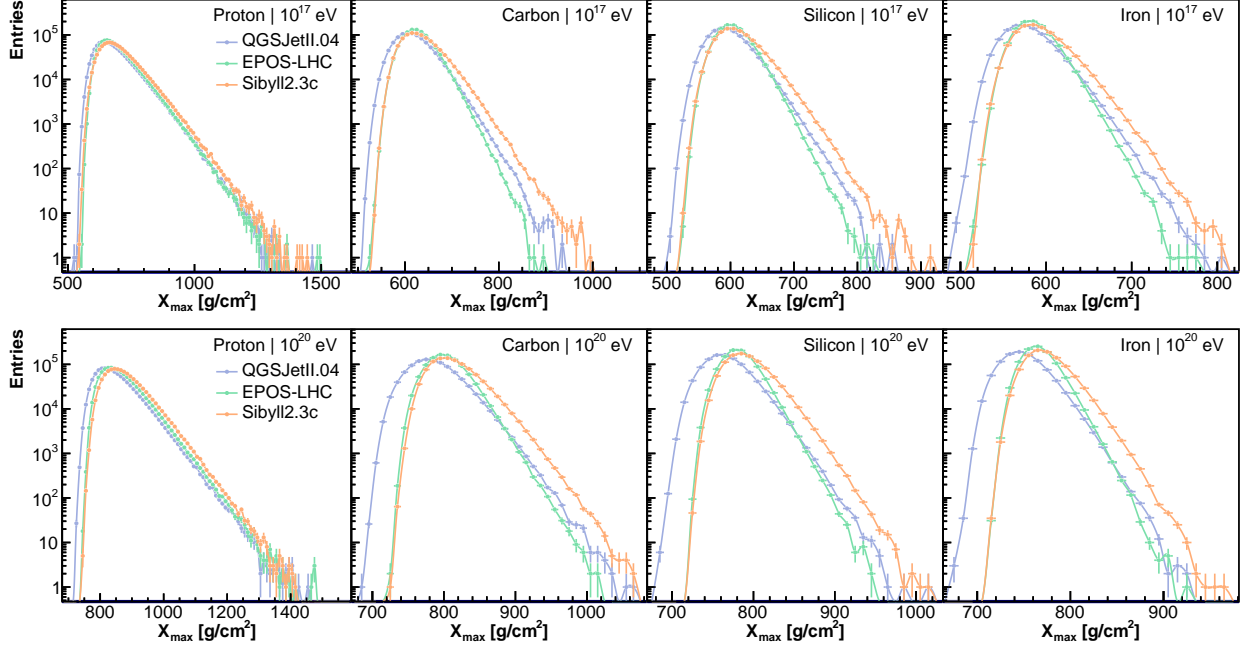


FIG. 1: Examples of simulated  $X_{\max}$  distributions for four different primary masses (proton, carbon, silicon, iron) and three hadronic interaction models (QGSJETII.04, EPOS-LHC and SIBYLL2.3c) at the energies  $10^{17}$  eV (upper panel) and  $10^{20}$  eV (lower panel).

### A. Exponentially Modified Gaussian distribution

The Exponentially Modified Gaussian (EMG) distribution was proposed in [6] to describe  $X_{\max}$  distributions. It is motivated by the assumption that  $X_{\max}$  can be decomposed as  $X_{\max} = X_{\text{first}} + \Delta X_{\max}$ , where  $X_{\text{first}}$  is the depth of the first interaction and  $\Delta X_{\max}$  represents the shower development after the first interaction. While  $X_{\text{first}}$  is known to have an exponential distribution with the mean free path  $\lambda$ , the distribution of  $\Delta X_{\max}$  is unknown. The simplest approach is to assume that  $\Delta X_{\max}$  is normally distributed with an average  $\mu$  and variance  $\sigma^2$ , so that  $X_{\max}$  is distributed according to the convolution of an exponential and a Gaussian. The resulting function is:

$$f(x) = \frac{1}{2\lambda} \exp\left(-\frac{x - \mu}{\lambda} + \frac{\sigma^2}{2\lambda^2}\right) \text{erfc}\left(\frac{\mu - x + \sigma^2/\lambda}{\sqrt{2}\sigma}\right), \quad (1)$$

where  $\text{erfc}(x)$  is the complementary error function.

The EMG has three parameters that can be interpreted in terms of extensive air showers physics.  $\lambda$ ,  $\mu$  and  $\sigma$  are related to the decay factor of the exponential, the depth of maximum

of the distribution and the width of the distribution, respectively.  $\sigma$  and  $\lambda$  influence both the width and the mean of the  $X_{\max}$  distribution in different ways, mathematically  $\langle X_{\max} \rangle = \mu + \lambda$  and  $\text{RMS}(X_{\max}) = \sqrt{\sigma^2 + \lambda^2}$ . The EMG function has already been employed in studies such as the determination of  $X_{\max}$  moments from Pierre Auger Observatory [1], the comparison between Pierre Auger Observatory and Telescope Array  $X_{\max}$  data [3] and the proposal of new methods to study the mass composition from real  $X_{\max}$  data [4].

## B. Generalized Gumbel distribution

The Gumbel distribution arises in the field of extreme value statistics to describe the frequency of extreme events (either minimum or maximum) in series of independent and identically distributed random variables [16]. The Generalized Gumbel distribution (GMB) [17] is written as

$$f(x) = \frac{1}{\sigma} \frac{\lambda^\lambda}{\Gamma(\lambda)} \exp \left\{ -\lambda \left[ \frac{x - \mu}{\sigma} + \exp \left( -\frac{x - \mu}{\sigma} \right) \right] \right\}. \quad (2)$$

Note that for  $\lambda = 1$  one recovers the standard Gumbel distribution. Equation 2 was proposed by reference [7] to describe  $X_{\max}$  distributions.

The importance of the GMB distribution in extreme value statistics and its relation with the statistics of sums [18] can give some insight on its use to describe the  $X_{\max}$  distribution. Suppose a series of random variables  $X_k$  is exponentially distributed according to

$$g_k(x) = \frac{\lambda + k}{\sigma} e^{-(\lambda+k)x/\sigma}. \quad (3)$$

It has been shown in reference [19] that the distribution of the sum  $\sum_{k=0}^{\infty} X_k$  converges exactly to equation 2 after a convenient shift and re-scaling of  $X_k$ . That is, the asymptotic sum of exponentially distributed random variables with increasing amplitudes converges to a GMB distribution. Based on it, it is possible to interpret  $X_{\max}$  as a sum of interaction depths of multiple generations of particles, similar to the model proposed in reference [20], but with variable interaction lengths, and to write

$$X_{\max} = \sum_{k=0}^{\eta-1} X_k, \quad (4)$$

where  $\eta$  is the number of generations of particles. If  $\eta \rightarrow \infty$  the distribution of the sum converges to equation 2. In this scenario, the mean free path of the first interaction is given by  $\sigma/\lambda$ . The scale parameter  $\sigma$  describes how fast the average interaction lengths change between generations of particles. The location parameter ( $\mu$ ) of equation 2 is introduced to shift the mean of the distribution.

For finite  $\eta$ , the sum above follows a beta-exponential distribution [21]:

$$f(x) = \frac{1}{\sigma B(\eta, \lambda)} e^{-\lambda x/\sigma} (1 - e^{-x/\sigma})^{\eta-1}, \quad (5)$$

where  $B(x, y)$  is the beta function, defined for  $x, y \geq 0$ . If a location parameter ( $\mu$ ) is added to the beta-exponential distribution, it could as well be considered a candidate to describe  $X_{\max}$  distributions. The beta-exponential distribution was also tested following the method explained below, however, it did not show any improvement in the description of  $X_{\max}$  distribution in comparison to the GMB. Since the beta-exponential function has one parameter more than the GMB, it was decided to keep only the GMB for further studies which in total has also three parameters.

### C. Log-normal distribution

The log-normal distribution is characteristic of stochastic processes where the variable of interest can be written as a product of independent and identically distributed random variables so that its logarithm is normally distributed according to the central limit theorem. The log-normal distribution (LOG) proves to be difficult to interpret in terms of extensive air showers. However, as it will be shown later, it provides a good description of  $X_{\max}$  distributions. The probability density function is given by

$$f(x) = \begin{cases} 0, & \text{if } x \leq m \\ \frac{1}{\sqrt{2\pi}\sigma} \frac{1}{x-m} \exp \left\{ -\frac{[\ln(x-m)-\mu]^2}{2\sigma^2} \right\}, & \text{if } x > m. \end{cases} \quad (6)$$

It has three parameters  $m$ ,  $\mu$  and  $\sigma$  related to the position of the peak, the width of the distribution and the length of the tail, respectively.

#### IV. FITTING THE $X_{\text{MAX}}$ DISTRIBUTIONS

The  $X_{\text{max}}$  distributions of each combination of primary mass, energy and hadronic interaction model are fitted using the three functions presented in the previous sections. The best description of the  $X_{\text{max}}$  distributions is achieved by searching for the three parameters in each function which resulted in the maximum likelihood. The  $X_{\text{max}}$  distributions are not binned (unbinned fit). The MINUIT [22] library available within the ROOT analysis framework [23] is used in the fitting procedure.

Examples of fitting results are presented in figure 2 for simulations obtained with QGSJETII.04 at an energy of  $10^{20}$  eV. Only for illustration purposes, the distributions are binned in intervals of  $10 \text{ g/cm}^2$ . Note the logarithmic scale in the y-axis. The primary particle is indicated at the top-right corner of each plot. Fit functions are shown as colored solid lines, while the simulated  $X_{\text{max}}$  distribution is shown as circular dots. The bottom panels show the deviation (pull values) of each fitted function to the simulated point, defined as the difference between the function and the point divided by the statistical uncertainty of the point.

Figure 2 shows that the EMG distribution is not able to describe the simulated distributions for small and large  $X_{\text{max}}$  values. No clear preference between the GMB and the LOG distributions is seen.

Values of the Akaike Information Criterion (AIC) for each case are shown in table I. Since the absolute value of the AIC has no meaning in this unbinned fit, the values shown are relative ( $\Delta_i$ ) to the smallest AIC in each case. Reader is referred to appendix A for the definition of AIC.

The first notable fact in table I is that the EMG distribution has the worst AIC value for every primary, energy and hadronic interaction model except one: silicon -  $10^{20}$  eV - EPOS-LHC for which the AIC value is slightly better than the GMB fit. This makes the EMG distribution the worst selection among the three functions described here to describe  $X_{\text{max}}$  distributions of single primary particles.

The GMB and LOG distributions represent similar good description of the  $X_{\text{max}}$  distributions. The LOG distribution performs better for low mass primaries (proton and carbon) and the GMB distribution performs better for heavier primaries (silicon and iron). But the differences between the quality of the fit of GMB and LOG are only marginal.



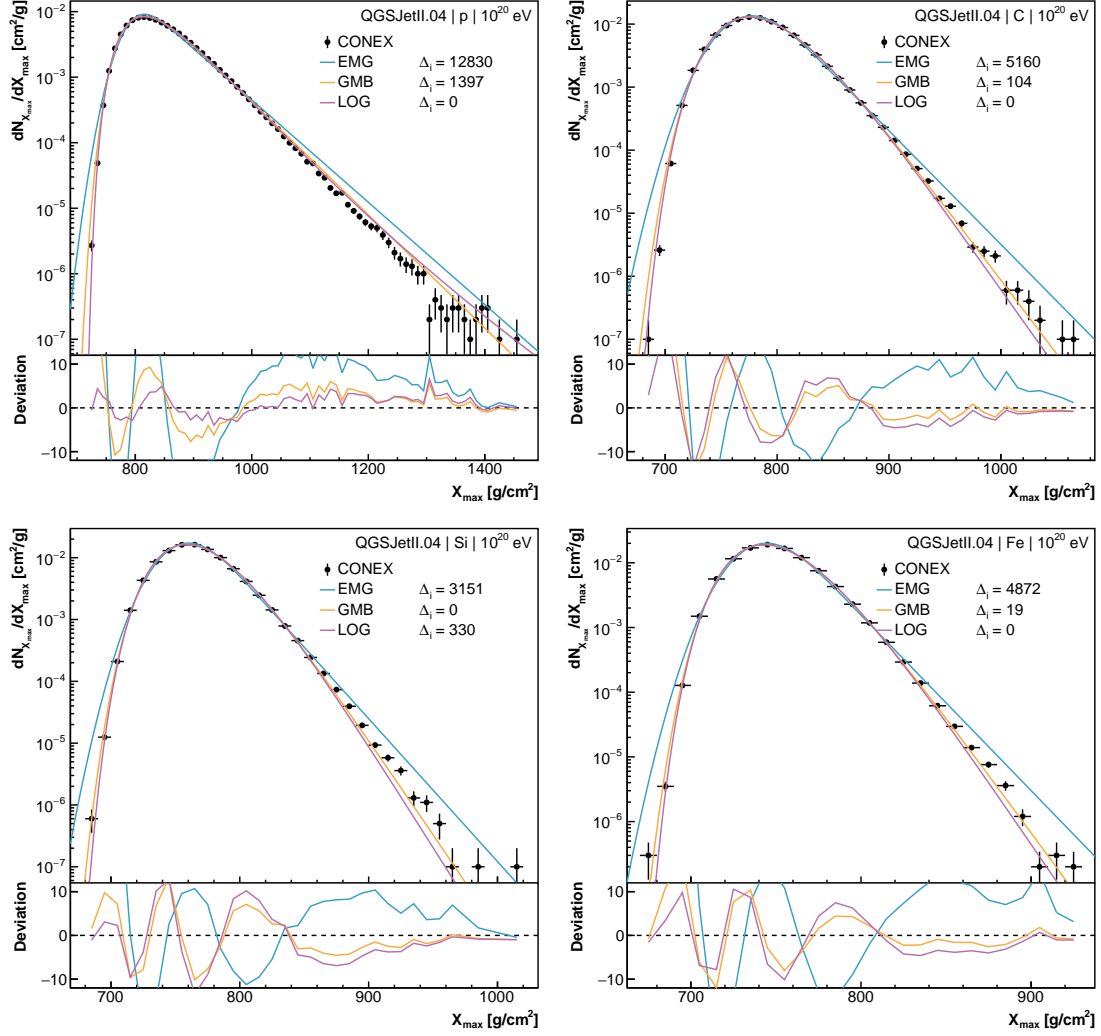


FIG. 2: Examples of fits of  $X_{\max}$  distributions. The primary particle is indicated at the top-right corner of each plot. Fit functions are shown as colored solid lines, while the simulated  $X_{\max}$  distribution is shown as circular dots. The bottom panels show the deviation of each fitted function to the simulated point, defined as the difference between the function and the point divided by the statistical uncertainty of the point. Only results for QGSJETII.04 are shown in this example.

### A. Mixed composition

The  $X_{\max}$  distributions of events with energy between  $10^{18}$  eV and  $10^{19}$  eV measured by the Pierre Auger Observatory can be better described by a combination of primary particles rather than a pure element [5, 24]. Therefore in the analysis of these distributions it is important that the used function is able to describe also mixed compositions instead of only

TABLE I: Relative AIC values ( $\Delta_i$ ) of the fit of the unbinned  $X_{\text{max}}$  distributions for the three hadronic interaction models and primary particle energy ranging from  $10^{17}$  eV to  $10^{20}$  eV. Note that a value of zero for a model means that this is the best model for the respective energy, mass and hadronic model combination.

QGSJETII.04																
Primary	Proton				Carbon				Silicon				Iron			
$\log(E_0/\text{eV})$	17	18	19	20	17	18	19	20	17	18	19	20	17	18	19	20
EMG	10113	11209	12226	12830	6636	6099	5181	5160	4213	3743	3447	3151	4920	5251	4875	4872
GMB	675	1044	1285	1397	131	105	32	104	0	0	0	0	0	0	0	19
LOG	0	0	0	0	0	0	0	0	402	381	384	330	202	79	81	0
EPOS-LHC																
EMG	8932	10507	13115	14264	4325	3884	3728	3027	2156	1236	1315	0	1742	1066	1571	1563
GMB	28	573	1425	1865	0	0	0	0	0	0	0	475	0	0	0	0
LOG	0	0	0	0	232	293	262	272	526	629	643	1222	681	754	781	802
SIBYLL2.3C																
EMG	9319	10117	11619	12648	11851	11493	11277	10987	6492	6637	6559	6269	6542	6282	5655	4954
GMB	420	666	1103	1362	914	805	760	713	0	0	0	0	0	0	0	0
LOG	0	0	0	0	0	0	0	0	247	182	123	139	326	379	495	538

pure samples. In this section, the proposed functions are going to be tested against a mix of primary particles. The simulated  $X_{\text{max}}$  distributions are mixed following the fraction which best describes the data of the Pierre Auger Observatory as shown in reference [5] and table II. Figure 3 shows two examples of mixtures at  $10^{18}$  eV for EPOS-LHC and SIBYLL2.3C models. Distributions are binned in intervals of  $10 \text{ g/cm}^2$  for illustration purposes. The resulting mixture is fitted by the three proposed functions.

The  $\Delta_i$  values for the fits are shown in table III. The GMB shows an overall better description of the distributions, losing only marginally to the EMG for EPOS-LHC at  $10^{18}$  eV and LOG for SIBYLL2.3C at  $10^{19}$  eV.

## V. PARAMETRIZATION OF $X_{\text{MAX}}$ DISTRIBUTIONS AS A FUNCTION OF ENERGY AND MASS

The three proposed functions are used to fit the simulated  $X_{\text{max}}$  distributions for proton, carbon, silicon and iron with energies ranging from  $10^{17}$  eV to  $10^{20}$  eV in steps of 1 in  $\log_{10}(E_0/\text{eV})$ . Each function has three parameters as shown in section III. These parameters are modeled as a function of primary energy and mass. The proposed functional form is:

Model	EPOS-LHC		QGSJETII.04		SIBYLL2.3C	
$\log(E_0/\text{eV})$	18	19	18	19	18	19
p	61.5%	9.5%	63.2%	35.6%	40.4%	2.8%
He	0.0%	62.0%	36.8%	64.4%	9.7%	38.7%
C	36.7%	28.5%	0.0%	0.0%	49.9%	58.5%
Fe	1.8%	0.0%	0.0%	0.0%	0.0%	0.0%

TABLE II: Primary fractions which best describes the  $X_{\text{max}}$  distributions measured by the Pierre Auger Observatory [5] at the energies used in this paper.

FIG. 3: Example of  $X_{\text{max}}$  distributions at an energy of  $10^{18}$  eV following the fractions shown in table II. Filled histograms with color lines represent the distribution of each primary particle. Black dots shows the sum of all particles. Color lines shows the result of the fit of proposed functions to the distribution of all particles (black dots). Left panel for EPOS-LHC and right panel for SIBYLL2.3C.

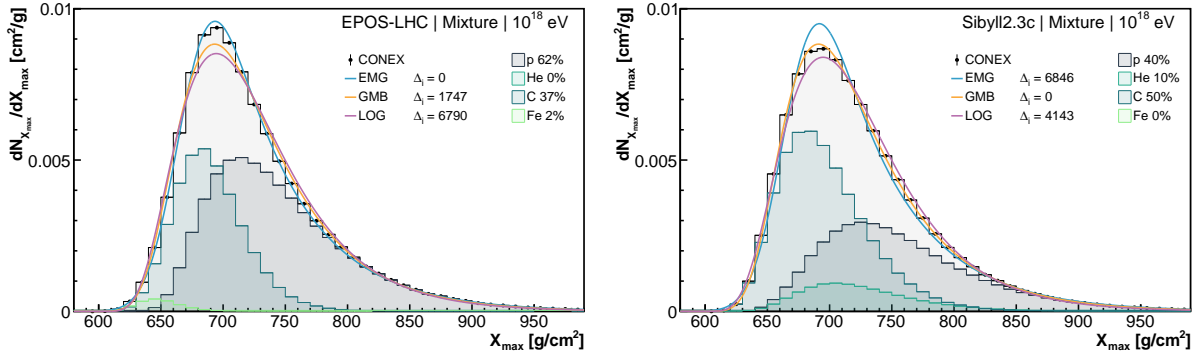


TABLE III: Relative AIC values ( $\Delta_i$ ) of the fit of the unbinned  $X_{\text{max}}$  distributions for the three hadronic interaction models and mix of primary particle. Note that a value of zero for a model means that this is the best model for the respective energy, mass and hadronic model combination.

Model	EPOS-LHC		QGSJETII.04		SIBYLL2.3C	
$\log(E_0/\text{eV})$	18	19	18	19	18	19
EMG	0	5557	6093	5415	6846	9378
GMB	1747	0	0	0	0	200
LOG	6790	991	4813	1457	4143	0

$$\theta(E_0, A) = a(A) + b(A) \log_{10} E_0 + c(A) (\log_{10} E_0)^2, \quad (7)$$

where

$$\begin{aligned} a(A) &= a_0 + a_1 \log_{10} A + a_2 (\log_{10} A)^2, \\ b(A) &= b_0 + b_1 \log_{10} A + b_2 (\log_{10} A)^2, \\ c(A) &= c_0 + c_1 \log_{10} A + c_2 (\log_{10} A)^2. \end{aligned} \quad (8)$$

Values obtained for the parameters  $a_i$ ,  $b_i$  and  $c_i$  and their corresponding statistical uncertainties are found in appendix B. Note that a value of zero in table IV means the inclusion of that parameters leads to a worse fit of the simulated distribution.

The error caused by the use of equations 7 and 8 to calculate the parameters as a function of mass and energy was determined by evaluating the differences between the first and second moments of the parametrized distributions and the simulated distributions for each mass and energy. Results are shown as histograms in figure 4. The upper plots show the deviations on the first moment of the  $X_{\max}$  distributions for each hadronic interaction model indicated in the top left corner of each box. The lower plots show the differences for the second moment of the  $X_{\max}$  distributions. The largest difference between the proposed parametrization and the simulations is  $2 \text{ g/cm}^2$  for the first moment and  $3 \text{ g/cm}^2$  for the second moment.

References [6] (Peixoto et al.) and [7] (de Domenico et al.) also proposed parametrizations of the  $X_{\max}$  distributions. The comparison of these parametrizations with the ones presented here is meaningful only when the same hadronic interaction models was used. Figure 5 compares first and second moments of the previously proposed parametrizations with the ones presented in this paper for simulations performed with QGSJETII.04 and EPOS-LHC hadronic interaction models. Previous parametrizations differs on the  $\langle X_{\max} \rangle$  by as much as  $20 \text{ g/cm}^2$  and on  $\text{RMS}(X_{\max})$  by as much as  $12 \text{ g/cm}^2$ .

## VI. CONCLUSION

The  $X_{\max}$  distribution is of great importance in UHECR studies and some functional forms have been proposed to describe it. In this paper, for the first time, three functions have been selected, explained, and compared to simulated  $X_{\max}$  distributions. A large

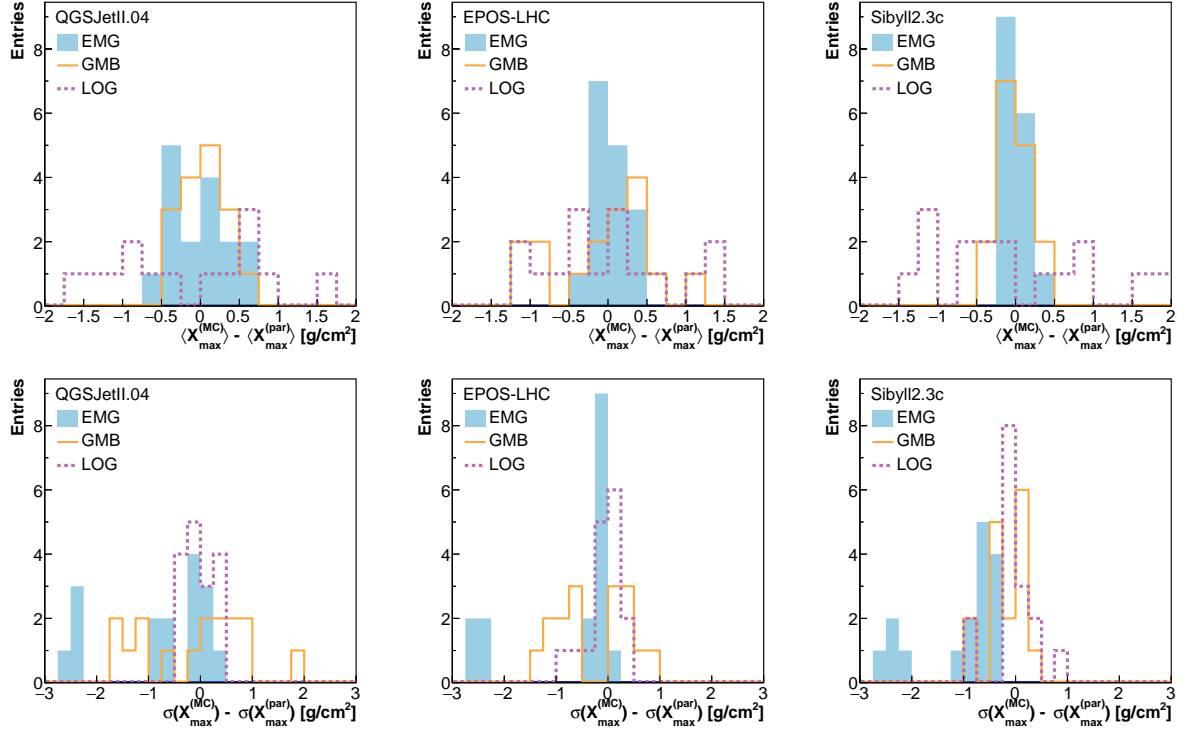


FIG. 4: Error on the first moment (upper plots) and second moment (lower plots) between the parametrized distributions (par) and the simulated (MC)  $X_{\max}$  distributions.

sample of showers ( $10^6$ ) has been generated for each point in a wide range of parameters space: four atomic nuclei have been considered: proton, carbon, silicon and iron with energies ranging from  $10^{17}$  eV to  $10^{20}$  eV and three hadronic interaction models: EPOS-LHC, QGSJETII.04, and SIBYLL2.3C. The primaries have also been mixed with fractions given by the best description of the Pierre Auger Observatory data.

In total three functions have been tested. Two were taken from the literature: Generalized Gumbel distribution [7] and Exponentially Modified Gaussian distribution [6], and, in addition, the Log-normal distribution has been used as well. All functions have three parameters. The parameters have been fitted to the simulated  $X_{\max}$  distributions and the result is shown in table IV. The excellent quality of the fits allows the prediction of the first and second moments of the  $X_{\max}$  distribution with a maximum error of 2 and 3  $g/cm^2$ , respectively.

The function that shows an overall best description of the  $X_{\max}$  distributions is the Generalized Gumbel distribution, followed by the Log-normal distribution. In some specific cases, the Log-normal distribution has a slightly better fit to the simulated distributions.

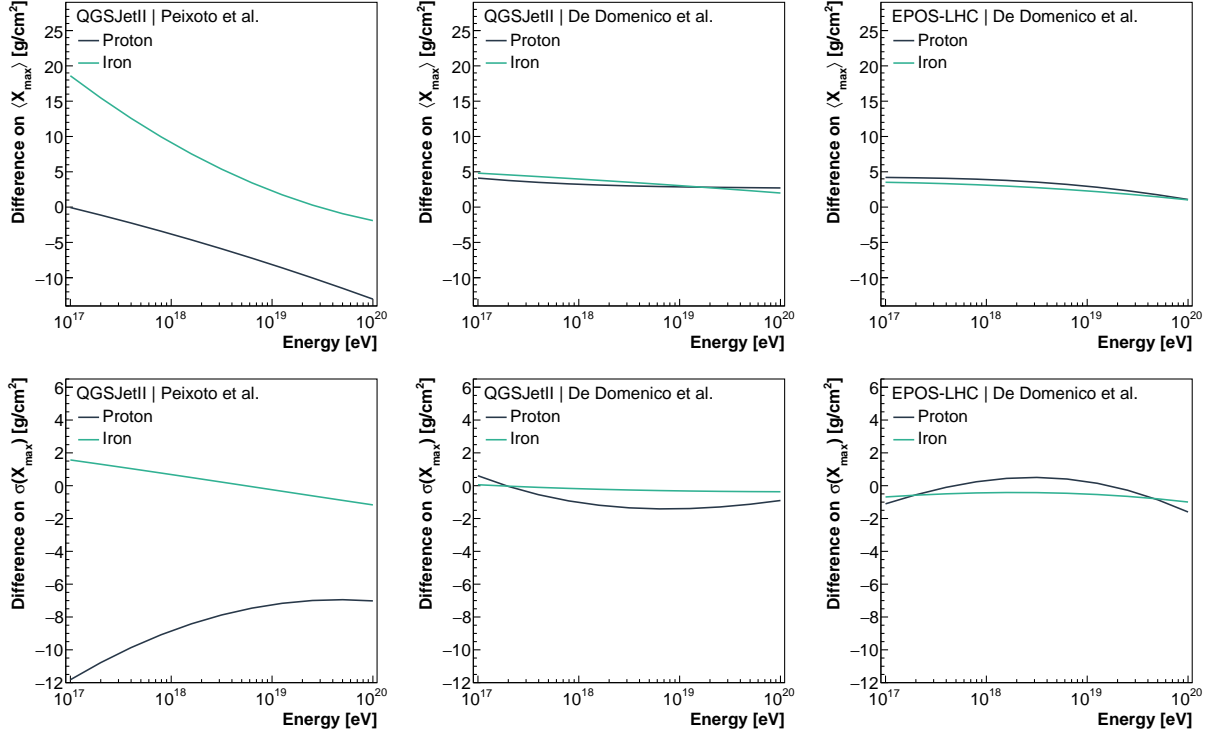


FIG. 5: Comparison between first (upper plots) and second (lower plots) moments of parametrized  $X_{\max}$  distributions with parametrizations from [6] (left) and [7] (middle and right). Results are shown only for parametrizations based on simulations with the same hadronic model, which is indicated in the top-left corner of each plot.

However, in many other cases, the Generalized Gumbel distribution is much better than the Log-normal distribution. In studies of measured  $X_{\max}$  distribution, it is not possible to know beforehand which is the primary particle. Moreover, the hadronic interaction model dependence of the analysis must be minimized. For those reasons, the Generalized Gumbel distribution is proposed here as the best choice because it shows the best description for most of the cases. The Exponentially Modified Gaussian distribution is the one which most poorly describes the simulated showers among the three functions studied for almost all cases.

## Acknowledgments

Authors acknowledge FAPESP Project 2015/15897-1. VdS acknowledge CNPq. This study was financed in part by the Coordenação de Aperfeiçoamento de Pessoal de Nível Su-

perior - Brasil (CAPES) - Finance Code 001. Authors acknowledge the National Laboratory for Scientific Computing (LNCC/MCTI, Brazil) for providing HPC resources of the SDumont supercomputer (<http://sdumont.lncc.br>). Thanks to Roger Clay and Michael Unger for reading and commenting the manuscript.

## A. AKAIKE INFORMATION CRITERION

The Akaike Information Criterion (AIC) [25, 26] is defined as

$$\text{AIC} = 2k - 2\log\left(\mathcal{L}(\vec{\theta})\right), \quad (9)$$

where  $k$  is the number of fitted parameters and  $\mathcal{L}$  is the maximized value of the likelihood function for the fitted parameter set  $\vec{\theta}$ . Given a set of models, the AIC criterion calculates the relative quality of each model in describing the data. From its definition, it is expected that the model with the smaller AIC value in a set is the one that has the smallest statistical distance to the data set used to fit model parameters.

Given that the absolute values of AIC carry no meaning and depend on the sample size, in this paper, model selection is based on the computation of the so-called Akaike differences ( $\Delta_i$ ), or relative AIC. These are defined as the AIC values of each model with respect to the model with the smaller AIC, that is,

$$\Delta_i = \text{AIC}_i - \text{AIC}_{\min}. \quad (10)$$

The relative AIC values provide a strong support for model selection in terms of information theory. A value of  $\Delta_i = 0$  means that a model is preferred among the set to describe fitted data. Small values of  $\Delta_i$  indicate that this model is not the best for the particular data set, but is competitive and should not be discarded. Large values of  $\Delta_i$ , on the other hand provide a strong argument against the  $i$ -th model.

## B. PARAMETER VALUES

In section V a method to describe the evolution of  $X_{\max}$  distributions energy and mass is proposed in terms of equations 7 and 8. This appendix compiles fitted parameters  $a_i$ ,  $b_i$  and  $c_i$  of equation 8. Table IV shows the values of fitted parameters whereas table V.

TABLE IV: Fitted parameters of equation 8 describing the evolution of  $X_{\text{max}}$  distributions as a function of primary energy and mass. Details in section V.

Exponentially modified gaussian									
QGSJetII.04	$a_1$	$a_2$	$a_3$	$b_1$	$b_2$	$b_3$	$c_1$	$c_2$	$c_3$
$\lambda$	391.6	-354.39	97.21	-31.848	31.654	-9.193	0.7526	-0.7955	0.2407
$\mu$	-544.3	-152.02	-33.81	76.067	17.644	1.251	-0.4692	-0.5436	0
$\sigma$	44.9	-2.7	-4.35	-1.03	0.25	0	0	0	0
EPOS-LHC	$a_1$	$a_2$	$a_3$	$b_1$	$b_2$	$b_3$	$c_1$	$c_2$	$c_3$
$\lambda$	478.15	-576.14	204.98	-41.845	55.499	-20.799	1.0336	-1.4561	0.5626
$\mu$	-757.99	-133.86	-32.58	99.306	15.373	0.914	-1.053	-0.4468	0
$\sigma$	239.07	-50.64	-18.25	-23.27	7.411	0.778	0.624	-0.2493	0
Sibyll2.3c	$a_1$	$a_2$	$a_3$	$b_1$	$b_2$	$b_3$	$c_1$	$c_2$	$c_3$
$\lambda$	389.8	-199.83	3.46	-31.021	16.28	0.168	0.7148	-0.3993	0
$\mu$	-784.86	-3.33	-15.91	100.993	-0.983	0.433	-1.0377	0	0
$\sigma$	80.76	8.01	-10.2	-4.684	-0.815	0.526	0.0988	0	0
Generalized Gumbel									
QGSJetII.04	$a_1$	$a_2$	$a_3$	$b_1$	$b_2$	$b_3$	$c_1$	$c_2$	$c_3$
$\lambda$	1.24	11.74	-6.85	-0.088	-1.393	0.855	0.00302	0.04702	-0.02778
$\mu$	-368.79	-238.75	-32.14	61.443	25.159	1.255	-0.1138	-0.7326	0
$\sigma$	55.9	20.9	-15.9	-1.08	0.32	0	0	0	0
EPOS-LHC	$a_1$	$a_2$	$a_3$	$b_1$	$b_2$	$b_3$	$c_1$	$c_2$	$c_3$
$\lambda$	4.34	-4.84	4.83	-0.4489	0.427	-0.314	0.01325	0	0
$\mu$	-565.11	-211.43	-36.32	82.199	22.453	1.288	-0.6189	-0.6475	0
$\sigma$	377.3	324	-228.1	-37.67	-29.63	22.436	1.0216	0.7366	-0.5955
Sibyll2.3c	$a_1$	$a_2$	$a_3$	$b_1$	$b_2$	$b_3$	$c_1$	$c_2$	$c_3$
$\lambda$	0.02	0.16	0.11	0.038	0.014	0	0	0	0
$\mu$	-537.61	-131.99	-19.68	78.952	11.515	0.731	-0.4886	-0.3366	0
$\sigma$	60	24	-17	-1.06	-1.5	0.78	0	0	0
Log-normal									
QGSJetII.04	$a_1$	$a_2$	$a_3$	$b_1$	$b_2$	$b_3$	$c_1$	$c_2$	$c_3$
$\mu$	8.974	-0.84	0.317	-0.3978	0.0684	-0.0344	0.0096	0	0
$\sigma$	0.532	-0.08	-0.04	-0.0065	-0.01	0.0066	0	0	0
$m$	-1152.4	64.9	-50	129.78	-8.74	4.65	-1.846	0	0
EPOS-LHC	$a_1$	$a_2$	$a_3$	$b_1$	$b_2$	$b_3$	$c_1$	$c_2$	$c_3$
$\mu$	14.745	-2.04	0.043	-1.058	0.2761	-0.023	0.02806	-0.00752	0
$\sigma$	0.034	-0.31	0.0043	0.0544	-0.00104	0.00582	-0.001768	0	0
$m$	-1745.1	-168.6	23.9	198.41	4.04	0.64	-3.738	0	0
Sibyll2.3c	$a_1$	$a_2$	$a_3$	$b_1$	$b_2$	$b_3$	$c_1$	$c_2$	$c_3$
$\mu$	5.78	-0.03	-0.059	-0.0422	-0.0094	0	0	0	0
$\sigma$	0.551	-0.151	0.014	-0.0086	0.0026	0	0	0	0
$m$	-1085.3	-66.4	24.2	120.33	2.68	-1.38	-1.493	0	0



TABLE V: Statistical uncertainty on fitted parameters of equation 8 describing the evolution of  $X_{\text{max}}$  distributions as a function of primary energy and mass. Details in section V.

Exponentially modified gaussian									
QGSJetII.04	$a_1$	$a_2$	$a_3$	$b_1$	$b_2$	$b_3$	$c_1$	$c_2$	$c_3$
$\lambda$	0.1	0.08	0.05	0.006	0.004	0.003	0.0003	0.0002	0.0001
$\mu$	0.1	0.08	0.05	0.006	0.005	0.003	0.0003	0.0002	0
$\sigma$	0.4	0.3	0.03	0.02	0.02	0	0	0	0
EPOS-LHC	$a_1$	$a_2$	$a_3$	$b_1$	$b_2$	$b_3$	$c_1$	$c_2$	$c_3$
$\lambda$	0.08	0.06	0.04	0.005	0.003	0.002	0.0002	0.0002	0.0001
$\mu$	0.08	0.06	0.04	0.005	0.004	0.002	0.0002	0.0002	0
$\sigma$	0.05	0.04	0.02	0.003	0.002	0.001	0.0002	0.0001	0
Sibyll2.3c	$a_1$	$a_2$	$a_3$	$b_1$	$b_2$	$b_3$	$c_1$	$c_2$	$c_3$
$\lambda$	0.1	0.08	0.04	0.006	0.004	0.002	0.0003	0.0002	0
$\mu$	0.1	0.07	0.04	0.006	0.004	0.002	0.0003	0	0
$\sigma$	0.07	0.05	0.03	0.004	0.003	0.002	0.0002	0	0
Generalized Gumbel									
QGSJetII.04	$a_1$	$a_2$	$a_3$	$b_1$	$b_2$	$b_3$	$c_1$	$c_2$	$c_3$
$\lambda$	0.01	0.03	0.02	0.0008	0.002	0.001	0.00003	0.00009	0.00006
$\mu$	0.09	0.06	0.04	0.005	0.004	0.002	0.0003	0.0002	0
$\sigma$	0.9	0.8	0.1	0.05	0.04	0	0	0	0
EPOS-LHC	$a_1$	$a_2$	$a_3$	$b_1$	$b_2$	$b_3$	$c_1$	$c_2$	$c_3$
$\lambda$	0.01	0.04	0.03	0.0009	0.002	0.001	0.00003	0	0
$\mu$	0.07	0.05	0.03	0.004	0.003	0.002	0.0002	0.0001	0
$\sigma$	0.2	0.2	0.1	0.02	0.01	0.008	0.0007	0.0006	0.0004
Sibyll2.3c	$a_1$	$a_2$	$a_3$	$b_1$	$b_2$	$b_3$	$c_1$	$c_2$	$c_3$
$\lambda$	0.03	0.04	0.007	0.001	0.002	0	0	0	0
$\mu$	0.08	0.06	0.04	0.005	0.004	0.002	0.0002	0.0002	0
$\sigma$	1	3	2	0.06	0.1	0.08	0	0	0
Log-normal									
QGSJetII.04	$a_1$	$a_2$	$a_3$	$b_1$	$b_2$	$b_3$	$c_1$	$c_2$	$c_3$
$\mu$	0.006	0.007	0.004	0.0004	0.0004	0.0002	0.00002	0	0
$\sigma$	0.007	0.02	0.01	0.0004	0.001	0.0006	0	0	0
$m$	0.7	0.8	0.5	0.05	0.04	0.03	0.002	0	0
EPOS-LHC	$a_1$	$a_2$	$a_3$	$b_1$	$b_2$	$b_3$	$c_1$	$c_2$	$c_3$
$\mu$	0.006	0.007	0.004	0.0004	0.0004	0.0002	0.00002	0.00002	0
$\sigma$	0.002	0.001	0.0009	0.0001	0.00007	0.00005	0.000005	0	0
$m$	0.6	0.7	0.4	0.04	0.04	0.02	0.002	0	0
Sibyll2.3c	$a_1$	$a_2$	$a_3$	$b_1$	$b_2$	$b_3$	$c_1$	$c_2$	$c_3$
$\mu$	0.02	0.02	0.002	0.0009	0.0008	0	0	0	0
$\sigma$	0.007	0.005	0.0007	0.0004	0.0003	0	0	0	0
$m$	0.6	0.5	0.3	0.04	0.03	0.02	0.002	0	0

### C. UPDATED PARAMETRIZATION

This section presents a parametrization analogous to that of appendix B, with the difference that helium-initiated showers were included in the simulation library used in the fit procedure. Table VI presents the fitted parameters and table VII shows the statistical uncertainties associated the parameters.

TABLE VI: Coefficients of the updated parametrization.

Exponentially modified gaussian									
QGSJetII.04	$a_1$	$a_2$	$a_3$	$b_1$	$b_2$	$b_3$	$c_1$	$c_2$	$c_3$
$\lambda$	383.46	-356.01	101.44	-30.988	31.724	-9.579	0.7286	-0.79657	0.25094
$\mu$	-574.89	-8.43	-111.97	79.455	2.183	9.633	-0.5610	-0.12668	-0.22589
$\sigma$	156.67	-60.67	0.29	-13.056	6.568	-0.5517	0.3234	-0.16979	0.01489
EPOS-LHC	$a_1$	$a_2$	$a_3$	$b_1$	$b_2$	$b_3$	$c_1$	$c_2$	$c_3$
$\lambda$	467.66	-570.44	205.90	-40.486	54.771	-20.9147	0.9920	-1.43480	0.56646
$\mu$	-751.27	-35.75	-96.00	98.577	4.680	7.8246	-1.03258	-0.15658	-0.18779
$\sigma$	261.54	-98.75	3.18	-25.563	12.681	-1.6304	0.68366	-0.39291	0.06668
Sibyll2.3c	$a_1$	$a_2$	$a_3$	$b_1$	$b_2$	$b_3$	$c_1$	$c_2$	$c_3$
$\lambda$	400.21	-298.36	61.12	-32.122	26.888	-6.048	0.7421	-0.68589	0.16888
$\mu$	-762.86	133.05	-115.19	98.588	-15.634	11.1213	-0.9698	0.39507	-0.28936
$\sigma$	103.77	17.05	-26.37	-7.208	-1.774	2.2770	0.16829	0.02605	-0.04786
Generalized Gumbel									
QGSJetII.04	$a_1$	$a_2$	$a_3$	$b_1$	$b_2$	$b_3$	$c_1$	$c_2$	$c_3$
$\lambda$	0.6465	1.932	1.767	-0.02109	-0.2143	-0.15658	0.001274	0.008431	0.004271
$\mu$	-412.77	-136.12	-76.789	66.4057	13.8397	6.1521	-0.24926	-0.42961	-0.12990
$\sigma$	211.50	-13.05	-13.36	-17.650	2.1148	0.8359	0.44432	-0.03287	-0.02996
EPOS-LHC	$a_1$	$a_2$	$a_3$	$b_1$	$b_2$	$b_3$	$c_1$	$c_2$	$c_3$
$\lambda$	5.621	4.614	-2.730	-0.5942	-0.5019	0.4506	0.017490	0.01506	-0.01395
$\mu$	-505.56	-356.03	27.79	75.805	38.127	-5.6766	-0.44325	-1.08321	0.19476
$\sigma$	446.23	-209.52	61.24	-45.209	27.790	-8.548	1.2330	-0.86067	0.26753
Sibyll2.3c	$a_1$	$a_2$	$a_3$	$b_1$	$b_2$	$b_3$	$c_1$	$c_2$	$c_3$
$\lambda$	-1.164	5.295	-1.288	0.1623	-0.5541	0.1595	-0.003128	0.015849	-0.004691
$\mu$	-608.46	58.10	-111.29	86.634	-9.002	10.606	-0.6925	0.21420	-0.26591
$\sigma$	123.53	100.69	-64.16	-8.066	-9.734	5.9116	0.1955	0.21773	-0.13790
Log-normal									
QGSJetII.04	$a_1$	$a_2$	$a_3$	$b_1$	$b_2$	$b_3$	$c_1$	$c_2$	$c_3$
$\mu$	7.4815	4.9797	-3.7692	-0.23720	-0.53973	0.394916	0.0053502	0.0150842	-0.0107345
$\sigma$	1.2503	-2.3907	1.1886	-0.08393	0.23658	-0.124054	0.0020535	-0.0063788	0.0033612
$m$	-838.51	-882.00	458.23	95.812	91.716	-49.171	-0.9373	-2.56672	1.36078
EPOS-LHC	$a_1$	$a_2$	$a_3$	$b_1$	$b_2$	$b_3$	$c_1$	$c_2$	$c_3$
$\mu$	14.6051	-9.7557	2.9011	-1.04208	1.13565	-0.350791	0.027637	-0.0321144	0.0098292
$\sigma$	-0.1712	0.9208	-0.1666	0.07662	-0.13820	0.027235	-0.0023838	0.0039718	-0.0007602
$m$	-1712.52	511.54	-184.49	194.863	-70.418	23.9702	-3.64482	2.11658	-0.70430
Sibyll2.3c	$a_1$	$a_2$	$a_3$	$b_1$	$b_2$	$b_3$	$c_1$	$c_2$	$c_3$
$\mu$	7.2028	0.5040	-1.0804	-0.19828	-0.06398	0.10976	0.004289	0.001508	-0.003020
$\sigma$	1.0921	-0.7835	0.3047	-0.06781	0.07805	-0.035924	0.0015989	-0.0022613	0.0011171
$m$	-985.13	-27.55	11.50	109.434	0.521	-1.363	-1.2006	-0.00453	0.04163

TABLE VII: Statistical uncertainties associated to the new set of coefficients.

Exponentially modified gaussian									
QGSJetII.04	$a_1$	$a_2$	$a_3$	$b_1$	$b_2$	$b_3$	$c_1$	$c_2$	$c_3$
$\lambda$	0.04	0.03	0.02	0.002	0.002	0.001	0.0001	0.00009	0.00005
$\mu$	0.04	0.03	0.02	0.002	0.002	0.001	0.0001	0.00009	0.00005
$\sigma$	0.04	0.03	0.02	0.002	0.002	0.0009	0.0001	0.00008	0.00005
EPOS-LHC	$a_1$	$a_2$	$a_3$	$b_1$	$b_2$	$b_3$	$c_1$	$c_2$	$c_3$
$\lambda$	0.03	0.02	0.02	0.002	0.001	0.0009	0.0001	0.00007	0.00004
$\mu$	0.03	0.02	0.02	0.002	0.001	0.0008	0.00009	0.00007	0.00004
$\sigma$	0.03	0.02	0.01	0.002	0.001	0.0008	0.00008	0.00006	0.00004
Sibyll2.3c	$a_1$	$a_2$	$a_3$	$b_1$	$b_2$	$b_3$	$c_1$	$c_2$	$c_3$
$\lambda$	0.04	0.03	0.02	0.002	0.002	0.001	0.0001	0.00008	0.00005
$\mu$	0.03	0.03	0.02	0.002	0.001	0.0009	0.0001	0.00007	0.00005
$\sigma$	0.03	0.02	0.01	0.002	0.001	0.0009	0.00008	0.00007	0.00004
Generalized Gumbel									
QGSJetII.04	$a_1$	$a_2$	$a_3$	$b_1$	$b_2$	$b_3$	$c_1$	$c_2$	$c_3$
$\lambda$	0.0009	0.002	0.001	0.00005	0.0001	0.00007	0.000003	0.000006	0.000005
$\mu$	0.02	0.01	0.008	0.0009	0.0007	0.0004	0.00005	0.00004	0.00002
$\sigma$	0.02	0.03	0.01	0.001	0.0008	0.0006	0.00005	0.00005	0.00006
EPOS-LHC	$a_1$	$a_2$	$a_3$	$b_1$	$b_2$	$b_3$	$c_1$	$c_2$	$c_3$
$\lambda$	0.002	0.004	0.004	0.0001	0.0003	0.0002	0.000006	0.00001	0.00001
$\mu$	0.03	0.02	0.01	0.002	0.001	0.0009	0.00009	0.00007	0.00004
$\sigma$	0.04	0.03	0.02	0.002	0.002	0.001	0.0001	0.00009	0.00006
Sibyll2.3c	$a_1$	$a_2$	$a_3$	$b_1$	$b_2$	$b_3$	$c_1$	$c_2$	$c_3$
$\lambda$	0.002	0.002	0.002	0.0001	0.0001	0.0001	0.000006	0.000007	0.000005
$\mu$	0.04	0.03	0.02	0.002	0.002	0.001	0.0001	0.00008	0.00005
$\sigma$	0.03	0.03	0.02	0.002	0.001	0.0009	0.0001	0.00008	0.00005
Log-normal									
QGSJetII.04	$a_1$	$a_2$	$a_3$	$b_1$	$b_2$	$b_3$	$c_1$	$c_2$	$c_3$
$\mu$	0.0003	0.0003	0.0002	0.00002	0.00001	0.000009	0.0000009	0.0000007	0.0000005
$\sigma$	0.0002	0.0002	0.0001	0.00001	0.00001	0.000006	0.0000006	0.0000005	0.0000003
$m$	0.04	0.03	0.02	0.002	0.002	0.001	0.0001	0.00009	0.00005
EPOS-LHC	$a_1$	$a_2$	$a_3$	$b_1$	$b_2$	$b_3$	$c_1$	$c_2$	$c_3$
$\mu$	0.0003	0.0002	0.0002	0.00002	0.00001	0.000009	0.000001	0.0000007	0.0000005
$\sigma$	0.0002	0.0002	0.0001	0.00001	0.00001	0.000006	0.0000006	0.0000005	0.0000003
$m$	0.03	0.03	0.02	0.002	0.001	0.0008	0.00009	0.00007	0.00004
Sibyll2.3c	$a_1$	$a_2$	$a_3$	$b_1$	$b_2$	$b_3$	$c_1$	$c_2$	$c_3$
$\mu$	0.0004	0.0003	0.0002	0.00002	0.00002	0.00001	0.000001	0.000001	0.000001
$\sigma$	0.0003	0.0002	0.0001	0.00002	0.00001	0.000008	0.0000008	0.0000006	0.0000004
$m$	0.04	0.03	0.02	0.002	0.002	0.001	0.0001	0.00008	0.00005

- 
- [1] A. Aab *et al.* [Pierre Auger Collaboration], Phys. Rev. D **90**, no. 12, 122005 (2014)
  - [2] R. U. Abbasi *et al.* [Telescope Array Collaboration], Astrophys. J. **858**, no. 2, 76 (2018).
  - [3] V. de Souza [Pierre Auger and Telescope Array Collaborations], PoS ICRC **2017**, 522 (2018).
  - [4] S. Blaess, J. A. Bellido and B. R. Dawson, arXiv:1803.02520 [astro-ph.HE].
  - [5] J. Bellido [Pierre Auger Collaboration], PoS ICRC **2017**, 506 (2018).
  - [6] C. J. Todero Peixoto, V. de Souza and J. A. Bellido, Astropart. Phys. **47**, 18 (2013).
  - [7] M. De Domenico, M. Settimo, S. Riggi and E. Bertin, JCAP **1307**, 050 (2013).
  - [8] T. Bergmann *et al.* Astropart. Phys. **26**, 420-432 (2007).
  - [9] R. Engel, D. Heck and T. Pierog. Annu. Rev. Nucl. Part. Sci. **61**, 467–89 (2011).
  - [10] R. D. Parsons *et al.* Astropart. Phys. **34**, 832-839 (2011).
  - [11] L. B. Arbeletche, V. P. Gonçalves and M. A. Muller, Int. J. Mod. Phys. A **33**, no. 26, 1850153 (2018)
  - [12] T. Pierog, Iu. Karpenko, J. M. Katzy, E. Yatsenko and K. Werner. Phys. Rev. C. **92**, 034906 (2015).
  - [13] S. Ostapchenko. Phys. Rev. D. **83**, 014018 (2011).
  - [14] A. Fedynitch, F. Riehn, R. Engel, T. K. Gaisser and T. Stanev, arXiv:1806.04140 [hep-ph].
  - [15] C. Baus, R. Engel, T. Pierog, R. Ulrich and M. Unger, Proc. of 32nd ICRC.
  - [16] E. J. Gumbel, Statistics of Extremes, Dover Pub. (2004).
  - [17] E. Bertin, Phys. Rev. Lett. **95**, no. 17, 170601, (2005)
  - [18] M. Clusel, E. Bertin, Int. J. Mod. Phys. B **22**, no. 20, 3313-3368 (2008).
  - [19] T. Antal, M. Droz, G. Györgyi and Z. Rácz, Phys. Rev. Lett. **87**, no. 24, 240601, (2001)
  - [20] J. Matthews, Astropart. Phys. **22**, 387 (2005).
  - [21] S. Nadajarah, S. Kotz, Reliability engineering & system safety **91**, no. 6 689-697, (2006)
  - [22] F. James and M. Roos, Comput. Phys. Commun. **10**, 343 (1975).
  - [23] R. Brun, and F. Rademakers, Nucl. Instrum. Meth. A **389**, 81 (1997).
  - [24] A. Aab *et al.* [Pierre Auger Collaboration], Phys. Rev. D **90**, no. 12, 122006 (2014)
  - [25] H. Akaike, Information theory as an extension of the maximum likelihood principle, in: B. N. Petrov, and F. Csaki, International Symposium on Information Theory, second ed., Akademiai Kiado, Budapest (1973).

- [26] K. P. Burnham, and D. R. Anderson, D. R., Model selection and inference: a practical information-theoretical approach, second ed., Springer-Verlag, New York (1998).